A MULTI-FIDELITY BAYESIAN FRAMEWORK FOR ROBUST SEISMIC FRAGILITY ANALYSIS

Giacomo Sevieri[1], Roberto Gentile[1,2], and Carmine Galasso[2,3]

[1] Department of Civil, Environmental and Geomatic Engineering, University College London, London, UK
[2] Institute for Risk and Disaster Reduction, University College London, London, UK
[3] Scuola Universitaria Superiore (IUSS) Pavia, Italy

Correspondence: Carmine Galasso, Department of Civil, Environmental and Geomatic Engineering, University College London, London, WC1E 6BT, England, UK. Email: c.galasso@ucl.ac.uk

Fragility analysis of structures via numerical methods involves a complex trade-off between the desired accuracy, the explicit consideration of uncertainties (both epistemic and aleatory) related to the numerical model, and the available computational performance. This paper introduces a framework for deriving numerical fragility relationships based on multi-fidelity non-linear models of the structure under investigation and response-analysis types. The proposed framework aims to reduce the computational burden while achieving a desired accuracy of the fragility estimates without neglecting aleatory and epistemic uncertainties. The proposed approach is an extension of the well-known robust fragility analysis framework. Different model classes, each characterised by increasing refinement, are used to define multi-fidelity polynomial expansions of the fragility model parameters. Each analysis result is then considered as a "new observation" in a Bayesian framework and used to update the coefficients of the polynomial expansions. An adaptive sampling algorithm is also proposed to improve the performance of the multi-fidelity framework further. Specifically, such an adaptive sampling algorithm relies on partitioning the sample space and the Kullback–Leibler divergence to find the optimal sampling path. The sample space partitioning allows an analyst to specify different criteria and parameters of the algorithm for different regions, thus further improving the performance of the procedure. The proposed approach is illustrated for an archetype reinforced concrete frame for which two model classes are developed/analysed: the simple lateral mechanism analysis (SLaMA), coupled with the capacity spectrum method, and non-linear dynamic analysis. Both model classes involve a cloud-based approach employing unscaled real (i.e. recorded) ground motions. The fragility relationships derived with the proposed procedure are finally compared to those calculated by using only the most advanced/high-fidelity model class, thus quantifying the performance of the proposed approach and highlighting further research needs.

KEYWORDS
Bayesian inference; general Polynomial Chaos Expansion; multi-fidelity model; Robust fragility.

INTRODUCTION

Building-level seismic fragility is quantitatively expressed as the conditional probability that a structure/structural type will reach or exceed a specified level of damage (or damage state, DS) for a given value of a considered earthquake-induced ground-motion intensity measure (IM). Only limited/poor-quality historical damage/loss data, often associated with heterogeneous seismic regions, are generally available; hence, numerical (or simulation-based) fragility analysis represents an attractive option for various applications (e.g. [1,2]). The numerical derivation of fragility relationships entails a complex trade-off between the desired accuracy, the explicit consideration of uncertainties (both epistemic and aleatory) related to the numerical model of the structure under investigation, and the available computational performance. When high-performance computing is not available and/or the focus is on regional seismic risk assessment (i.e. for building portfolios of various sizes), simplified models are often adopted and/or epistemic uncertainties related to the model parameters neglected. The use of simplified models may lead to biased fragility (and consequently risk) estimates, notably when collapse fragility (and risk) is of interest. In addition, quantifying the impact on seismic fragility of 1) epistemic uncertainties due to structure-specific modelling parameters (e.g. material properties, structural detailing, considered capacity models; e.g. [3]), particularly in the case of existing buildings, e.g. [4]; 2) building-to-building variability within a structural type, particularly in seismic fragility/vulnerability modelling of building classes for portfolio risk assessment (e.g. [5]), is a crucial issue in many practical risk-assessment applications.

Sampling-based approaches (e.g. plain Monte Carlo, Latin Hypercube Sampling, among others) have been widely used to derive seismic fragility relationships considering both aleatory (i.e. record-to-record variability) and epistemic

uncertainties (i.e. related to the numerical model parameters or building-to-building variability within a structural type/building class). Several approaches have been proposed in the scientific literature to reduce the computational burden required in numerical fragility analysis. Most of these approaches combine non-linear dynamic analysis procedures based on recorded ground motions (e.g. incremental dynamic analysis, or IDA [6]; cloud analysis [7] with reliability methods, such as first-order second-moment (FOSM), also referenced as mean value first-order second-moment (MVFOSM; e.g. [8]) or response surface methods, e.g. [9]. Although these methods reduce the computational burden in the fragility derivation, they may suffer different drawbacks. In fact, the approximation error of response surfaces/statistical surrogate models is generally high in the region of the tails of the parameter distributions. This may lead to a poor approximation of the limit state function for a given DS. This issue is especially evident when the collapse DS is considered. In addition, approximated reliability methods may experience convergence issues, particularly when non-asymptotic problems are investigated [10]. Gradient-based methods may not correctly represent the interaction between uncertainties and, consequently, how they affect model outputs. For all the previous approaches, the accuracy of the calculation can be improved by increasing the number of samples or by applying more advanced computational strategies (e.g. subset simulation or importance sampling [11]).

An alternative way of dealing with seismic fragility derivation is to consider structural-analysis results related to a specific suite of ground-motion records and a set of model parameter realisations as observations within a Bayesian framework [12]. In this approach, known as robust fragility (RF, [7]), the fragility model parameters are treated as random variables and updated through the application of the Bayes rule. The RF approach has been successfully applied in conjunction with cloud-based non-linear dynamic analysis [13], which can also account for collapse cases (e.g. non-convergence of the analysis, likely corresponding to a plastic mechanism; unrealistically large values of the considered engineering demand parameter, EDP [7]. This approach is particularly convenient from a computational perspective and represents a recent fundamental improvement in the research field. However, in its current form, solutions derived from numerical models with different levels of accuracy cannot be readily combined. In other words, a specific numerical model/analysis type must be selected a priori, assessing the accuracy of the results and computational burden. Employing a set of numerical models characterised by different refinement levels would enable a more agile control of the trade-off between result accuracy and computational burden, particularly when solutions of simplified numerical models agree well with those of more refined ones (e.g. [14]).

This paper introduces a Bayesian framework for the derivation of numerical fragility relationships based on multi-fidelity models. The proposed framework can be regarded as a modification/extension of the current RF approach. The motivating idea is that, in the context of structural reliability/fragility analysis, high accuracy in the estimation of the structural performance is mostly required in the proximity of the DSs of interest. Therefore, the computational burden related to fragility derivation can be reduced by analysing refined structural models only when the structure is approaching a DS (i.e. when it is strictly necessary). In contrast, simplified or less-refined models can be used to evaluate the structural performance both in the safety and in the failure region of the probability space, far enough from the considered damage state. In the proposed approach, different model classes, each characterised by an increasing refinement, are used to surrogate the fragility model parameters through the general Polynomial Chaos Expansion (gPCE) technique [15]. Each analysis result is considered a "new observation" in the proposed Bayesian framework and used to update the gPCE coefficients. For the sake of simplicity, the proposed framework for fragility analysis is referred to as the gPCE-based multi-fidelity robust fragility (gPCE-MFRF) approach. An adaptive sampling strategy specifically defined for the gPCE-MFRF is also presented to further reduce the computational cost in the fragility-relationship derivation. The proposed adaptive sampling, based on a partitioning of the sample space, relies on the Kullback–Leibler divergence ($D_{KL}(\cdot)$) [16] for the selection of the sampling pattern. The gPCE-MFRF approach can be easily combined with different non-linear demand estimation methods for probability-based seismic assessment (e.g. [17]), such as cloud analysis. In this way, as for the case of RF, the uncertainty related to the IM variability (i.e. record-to-record variability) is considered in the calculation.

The proposed approach contributes to the research field of numerical methods for structural reliability analysis. The main advance of the proposed approach is the use of a multi-fidelity gPCE of the fragility model parameters, enabling the use of structural models with varying accuracy. The use of surrogate models in earthquake engineering and structural reliability analysis dates back to the 1990s. Ghanem and Spanos [18] provided a comprehensive viewpoint, up to that time, on this topic, thus paving the way for future research. Numerical integration or simulation-based approaches have been frequently used to calculate the probability of failure (or the reliability) of a structure. In this context, surrogate models (or metamodels) have been used to mimic the behaviour of a complex system (the simulator, i.e. a finite element model of a structure under consideration) by predicting the value of the target/output variable(s)

given a combination of the input variables. In other words, a statistical model is adopted to surrogate the relationship between inputs and outputs such that it is possible to make predictions for any input vector while remaining computationally cheap to evaluate. Various approaches have been proposed to build accurate surrogate models for the solutions of numerical structural analyses (e.g. for EDP estimation), always using a lower number of analyses (e.g. [19–22]). Similarly, accurate surrogate models have been proposed for the seismic fragility parameters (i.e. median and dispersion). For instance, Wang et al. [23] built an artificial neural network (ANN) to surrogate the output of a high-fidelity numerical model of a nuclear power plant under seismic action. The surrogate model is then used for the derivation of fragility curves. A forward selection approach is proposed to identify the most relevant ground-motion IMs for the AAN training based on semi-partial correlation coefficients, thus reducing the computational cost. Gentile and Galasso [5] proposed using Gaussian process regressions to surrogate the seismic fragility of building classes. This enables an analyst to efficiently account for building-to-building variability in simulation-based seismic risk assessment of building portfolios. Abbiati et al. [24] have recently proposed a computational framework for seismic fragility analysis based on a combination of synthetic ground motion, polynomial chaos-based global sensitivity analysis, and hierarchical kriging surrogate modelling. Specifically, a low fidelity numerical model of the structure under investigation, subjected to simulated ground motions, is used to build a gPCE-based proxy model for target EDPs. A global sensitivity analysis of the gPCE-based proxy model is then performed to identify the input parameters contributing most to the model output variability. Only these selected input parameters are considered as random variables in the seismic analysis of a high-fidelity numerical model of the structure. Finally, the gPCE-based proxy model results and those of the high-fidelity model are combined to create a hierarchical Kriging surrogate model of the target EDP, which is ultimately used to derive fragility curves. The approach proposed in this paper belongs to this latter category of surrogate models, making use of different model classes to surrogate the fragility model parameters. This leads to a further reduction of the computational burden as high-fidelity models are analysed only when strictly necessary.

The paper starts with a detailed presentation of the proposed framework, followed by an illustrative case study to show the feasibility of the proposed approach in practice. Particularly, two analysis refinement levels are considered for an archetype reinforced concrete (RC) frame building - although the proposed gPCE-MFRF can be applied with any number of model classes. The lowest refinement level is based on the Simple Lateral Mechanism Analysis (SLaMA) approach [25], a mechanics-based, analytical method that allows one to define the non-linear static force-displacement capacity and the plastic mechanism of RC structures. The highest refinement level relies on a detailed numerical model analysed through non-linear dynamic analysis. Fragility relationships are derived through a cloud-based approach employing unscaled real (i.e. recorded) ground motions and using the capacity spectrum method for SLaMA (using the same records). The fragility relationships derived with the proposed procedure are compared with those calculated using only the most advanced/high-fidelity model class. The results of the comparison are critically discussed. A sensitivity analysis of the number of samples adopted in the proposed framework is finally performed to provide comprehensive insights into the performance of the proposed approach and guide its practical implementations.

MULTI-FIDELITY SURROGATE FRAGILITY MODEL

The proposed approach, inspired by the concept of RF, relies on a multi-fidelity gPCE of the fragility model parameters (e.g. median, dispersion) to combine EDP (numerical) estimates calculated with different model classes. As in the case of RF, in the proposed approach, each fragility model parameter is described through a probability density function (PDF) rather than a deterministic value/point estimate. These random fragility model parameters act as proxies for the uncertainties in the numerical model (e.g. geometry, material properties), both epistemic and aleatory, which are then considered in the fragility relationship calculation. The structural model results ($\mathbf{y}$, e.g. in terms of seismic demand-to-capacity ratio, or *DCR*) are used in the proposed approach to updating the coefficients of the multi-fidelity gPCE of the fragility model parameters ($\boldsymbol{\chi}$). This peculiarity is a crucial difference between the proposed gPCE-MFRF approach and the RF one, in which the parameters $\boldsymbol{\chi}$ are directly updated in a Bayesian scheme. The multi-fidelity gPCE has a dual purpose: combining solutions of different model classes and expanding a random variable, thus reducing the computational burden needed to propagate uncertainties through deterministic models.

Figure 1 shows the main steps needed for applying the proposed gPCE-MFRF method, which is flexible enough to enable the use of different sampling approaches. The illustrative application presented/discussed in this paper demonstrates how the proposed adaptive sampling algorithm can effectively reduce the computational burden.

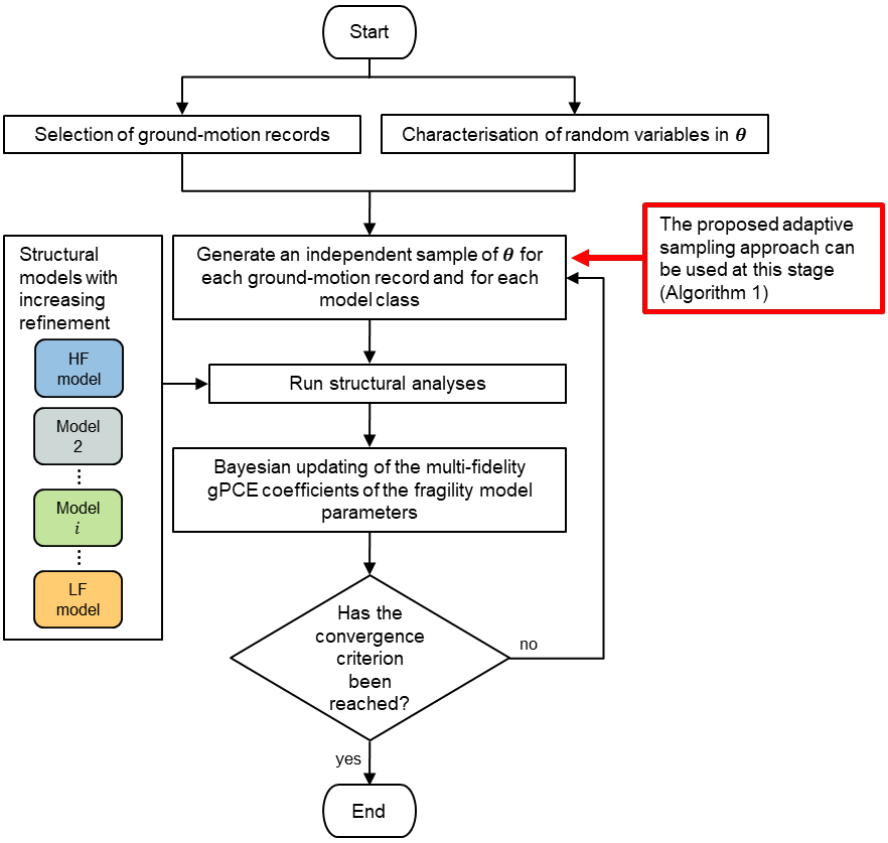

Figure 1 Flowchart of the gPCE-MFRF method: $\boldsymbol{\theta}$ is the vector of uncertain model parameters.

gPCE-based robust fragility

In its current version, the RF approach considers a fragility relationship for a given DS, $P\left(DCR_{DS_i} > 1|IM, \boldsymbol{\chi}\right)$, as the expected value of a prescribed fragility model over the posterior distribution, $f(\boldsymbol{\chi}|\mathbf{y})$, of the fragility model parameters ($\boldsymbol{\chi}$) conditioned on ($\mathbf{y}$):

$$P\left(DCR_{DS_i} > 1|IM, \mathbf{y}\right) = \int_{\Omega_{\chi}} P\left(DCR_{DS_i} > 1|IM, \boldsymbol{\chi}\right) f(\boldsymbol{\chi}|\mathbf{y})\, d\boldsymbol{\chi} = \mathbb{E}_{\boldsymbol{\chi}|\mathbf{y}}\left[P\left(DCR_{DS_i} > 1|IM, \boldsymbol{\chi}\right)\right]. \quad (1)$$

In Equation 1, DCR_{DS_i} is the demand-to-capacity ratio related to the i-th DS (for instance, in terms of maximum interstory drift ratio), IM is the ground-motion intensity measure considered in the fragility model and Ω_{χ} is the probability space where the fragility model parameters are defined (i.e. their support).

In the approach proposed in this study, Equation 1 is still valid, but the fragility model parameters collected in $\boldsymbol{\chi}$ are approximated through their multi-fidelity gPCE ($\boldsymbol{\chi}_{\mathrm{gPCE-MFRF}}$). Therefore, $f(\boldsymbol{\chi}|\mathbf{y})$ is replaced with $f\left(\boldsymbol{\chi}_{\mathrm{gPCE-MFRF}}|\mathbf{y}\right)$, which can be written in terms of the combination coefficients of the multi-fidelity gPCE, as shown in the next sections. In the context of a random variable expansion (e.g. gPCE of $\boldsymbol{\chi}_{\mathrm{gPCE-MFRF}}$), calibrating the combination coefficients in a Bayesian setting (concerning some available reference results $\mathbf{y}$) consists of determining the posterior distribution $f\left(\boldsymbol{\chi}_{\mathrm{gPCE-MFRF}}|\mathbf{y}\right)$ [26].

Once a reliable multi-fidelity gPCE is built, any consideration for the RF results is still valid for the proposed approach. Particularly, the uncertainty in the fragility model is due to both uncertainty effects [27] and sample size. The sample path dimension must be carefully calibrated to balance the accuracy of the results and the computational burden. The

accuracy of the developed fragility model can be assessed by calculating confidence intervals of the resulting fragility relationship.

For the sake of clarity and without loss of generality, the proposed approach is presented in this Section for the case of a fragility model, which explicitly considers the collapse cases [28]. The set of analysis results ($\mathbf{y}$) is portioned into two groups: 1) NoC data, for which the structure does not experience collapse; 2) C data, corresponding to collapse-inducing analysis cases. In this context, collapse-inducing analysis results can be related to the occurrence of very large DCR_{DS_i} values or nonconvergence in the analysing software, likely corresponding to a plastic mechanism (i.e. the structure is underdetermined). By applying the total probability theorem, the structural fragility for the i-th DS can be written as,

$$P\left(DCR_{DS_i} > 1|IM, \mathbf{y}\right) = P\left(DCR_{DS_i} > 1|IM, NoC\right)\left(1 - P(C|IM)\right) + P\left(DCR_{DS_i} > 1|IM, C\right)P(C|IM). \quad (2)$$

Assuming that $P\left(DCR_{DS_i} > 1|IM, NoC\right)$ is described by a lognormal distribution and that the probability of collapse $P(C|IM)$ is predicted by a logistic regression model [29] as a function of the considered IM, then the fragility model $P\left(DCR_{DS_i} > 1|IM, \boldsymbol{\chi}_{\mathrm{MFRF}}\right)$ can be expressed as:

$$P\left(DCR_{DS_i} > 1|IM, \boldsymbol{\chi}_{\mathrm{MFRF}}\right) = \Phi\left(\frac{\ln\left(im/\eta_{DS_i}^{\mathrm{MFRF}}\right)}{\beta_{DS_i}^{\mathrm{MFRF}}}\right)\frac{\exp\left(-\gamma^{\mathrm{MFRF}}(\ln IM)\right)}{1+\exp\left(-\gamma^{\mathrm{MFRF}}(\ln IM)\right)} + \frac{1}{1+\exp\left(-\gamma^{\mathrm{MFRF}}(\ln IM)\right)}. \quad (3)$$

In Equation 3, $\eta_{DS_i}^{\mathrm{MFRF}}$ and $\beta_{DS_i}^{\mathrm{MFRF}}$ are the multi-fidelity gPCE of the median and standard deviation of the fragility model for the NoC portion of $\mathbf{y}$; $\Phi(\cdot)$ is the standard normal cumulative distribution function; $\gamma^{\mathrm{MFRF}}(\ln IM)$ is the logit function [29] of the logistic model adopted for the collapse data. It is worth noting that, in this framework, $P\left(DCR_{DS_i} > 1|IM, \mathbf{y}\right)$ is equivalent to $P\left(DCR_{DS_i} > 1|IM, \boldsymbol{\chi}_{\mathrm{MFRF}}\right)$ as new analysis results ($\mathbf{y}$) are used in a Bayesian setting to update the distribution of the parameters collected in $\boldsymbol{\chi}_{\mathrm{MFRF}}$.

The vector of the fragility model parameters is $\boldsymbol{\chi}_{\mathrm{MFRF}} = \left[\ln\eta_{DS_i}^{\mathrm{MFRF}}, \beta_{DS_i}^{\mathrm{MFRF}}, \gamma^{\mathrm{MFRF}}(\ln IM)\right]$. In the parametrization of the fragility model (Equation 2), the logit function is written in a general form ($\gamma^{\mathrm{MFRF}}(\ln IM)$) rather than as the common linear model, usually adopted in the scientific literature for cloud analysis with collapse data [7]. In fact, in the proposed approach $\gamma(\ln IM)$ is approximated through its multi-fidelity gPCE. Therefore, using a linear model with the coefficient distributions approximated with the gPCE would lead to the same result. However, $\gamma(\ln IM)$ is still a logit function with only one predictor, i.e. $\ln IM$.

Multi-fidelity surrogate model based on the general Polynomial Chaos Expansion

The gPCE is a spectral method for propagating uncertainties ($\boldsymbol{\theta}$) through deterministic models [15]. In the context of stochastic modelling, this approach relies on orthogonal basis functions for the expansion of the PDF of an uncertain quantity of interest ($u(\boldsymbol{\theta})$, i.e. fragility model parameters or *DCRs* for different model classes in this study) resulting from the solution of the forward problem (i.e. propagation of uncertainties through a deterministic numerical model). In the specific application considered in this study, more than one quantity of interest is considered, i.e. the fragility model parameters collected in $\boldsymbol{\chi}_{\mathrm{MFRF}}$. As discussed above, the uncertainty parameters in $\boldsymbol{\theta}$, which lead to variability of the numerical output, may be related to class-specific attributes (e.g. geometry, material properties, structural detailing) governing the building-to-building variability or structure-specific ones (e.g. geometry, material properties, modelling assumptions) governing the within-building variability. For a given model class, the gPCE also provides a response surface ($\hat{u}_N$) that can be used to surrogate the model output in optimisation [30] or fragility [9] problems, as well as for the definition of probabilistic predictive models for structural health monitoring (e.g. [31]). Once a reliable gPCE is developed (i.e. gPCE with small approximation error), this technique allows one to solve the forward problem directly, as well as to perform variance-based sensitivity analysis [32] without any additional computational cost [33].

The gPCE is defined as an extension of the polynomial decomposition ([34] of $u(\boldsymbol{\theta})$:

$$u(\boldsymbol{\theta}) \approx \hat{u}_N(\boldsymbol{\theta}) = \sum_{|\mathbf{i}|\leq N} b_{\mathbf{i}}\,\psi_{\mathbf{i}}(\boldsymbol{\theta}), \quad (4)$$

where N is the cardinality of the polynomial expansion, $\mathbf{i}$ is a finite multi-index set, $\psi_{\mathbf{i}}(\boldsymbol{\theta})$ is the $\mathbf{i}$-th orthogonal basis function, $b_{\mathbf{i}}$ is the corresponding combination coefficient. The selection of the orthogonal basis functions is based on the PDF of the random parameters $\boldsymbol{\theta}$ [15]. In contrast, the calculation of the combination coefficients is based on some reference solutions of the deterministic model through interpolation, regression or the Bayesian approach [26]. The truncation scheme of the polynomial expansion must be selected to balance accuracy and overfitting issues.

The orthogonality property of the basis functions enables the mean value ($\mathbb{E}[u(\boldsymbol{\theta})]$) and variance ($\mathrm{VAR}[u(\boldsymbol{\theta})]$) of the uncertain model output $u(\boldsymbol{\theta})$ to be calculated as

$$\mathbb{E}[u(\boldsymbol{\theta})] \approx \mathbb{E}[\hat{u}_N(\boldsymbol{\theta})] = \int_{\Omega} \sum_{|\mathbf{i}|\leq N} b_{\mathbf{i}}\, \psi_{\mathbf{i}}(\boldsymbol{\theta})\, dF(\boldsymbol{\theta}) = b_{\mathbf{0}}, \tag{5}$$

$$\mathrm{VAR}[u(\boldsymbol{\theta})] \approx \mathrm{VAR}[\hat{u}_N(\boldsymbol{\theta})] = \sum_{0<|\mathbf{i}|\leq N} \varrho_{\mathbf{i}}\, b_{\mathbf{i}}^2. \tag{6}$$

In the Equations 5 and 6, Ω is the sample space of $\boldsymbol{\theta}$, $F(\boldsymbol{\theta})$ is the joint cumulative distribution function (CDF) of the model parameters, while $\varrho_{\mathbf{i}} = \mathbb{E}[\psi_{\mathbf{i}}^2(\boldsymbol{\theta})]$ are normalization factors.

Similarly, the partial variance of the model output related to the i-th random variable ($\mathrm{VAR}_i[u(\boldsymbol{\theta})]$) can be approximated through the gPCE. In this case, a sub-set $\mathbf{j}$ of $\mathbf{i}$, defined in such a way that only the indices related to the i-th random variable are considered, is used for the calculation of the variance:

$$\mathrm{VAR}_i[u(\boldsymbol{\theta})] \approx \mathrm{VAR}_i[\hat{u}_N(\boldsymbol{\theta})] = \sum_{\boldsymbol{\alpha}\in\mathbf{j}} \gamma_{\boldsymbol{\alpha}}\, b_{\boldsymbol{\alpha}}^2. \tag{7}$$

Total and partial variances are finally combined to derive the gPCE approximation of the Sobol' indices S_i,

$$S_i\big(u(\boldsymbol{\theta})\big) \approx S_i\big(\hat{u}_N(\boldsymbol{\theta})\big) = \frac{\mathrm{VAR}_i[\hat{u}_N(\boldsymbol{\theta})]}{\mathrm{VAR}[\hat{u}_N(\boldsymbol{\theta})]}. \tag{8}$$

The Sobol' indices represent a decomposition of the model output variance into fractions related to input parameters or set of them. They express how the variability of a particular input parameter, or a set of them, affects the total variability of the output. This sensitivity analysis approach does not require any linearity or monotonicity in the model, and it is completely defined in a probabilistic framework [32]. It is worth noting that the calculation of Sobol' indices through sampling-based methods is computationally expensive, and approximations are usually derived. The gPCE-based procedure presented above does not require any approximation of the Sobol' indices or additional computational cost as they are computed through algebraic calculations involving the gPCE coefficients [33].

Finally, the gPCE coefficients of the model outputs calculated for different model classes are combined to obtain a unique multi-fidelity gPCE. Let us assume that $\hat{u}_N^{\mathrm{HF}}(\boldsymbol{\theta})$ is the gPCE of an unknown quantity of interest related to the high-fidelity (HF) model ($u^{\mathrm{HF}}(\boldsymbol{\theta})$); $\hat{u}_N^{\mathrm{HF}}(\boldsymbol{\theta})$ is approximated through a multi-fidelity model $\hat{u}_N^{\mathrm{MF}}(\boldsymbol{\theta})$ composed of M low-fidelity (LF) model classes ($\hat{u}_N^{\mathrm{LF},j}(\boldsymbol{\theta})$) with lower accuracy, that is,

$$\hat{u}_N^{\mathrm{HF}}(\boldsymbol{\theta}) \approx \hat{u}_N^{\mathrm{MF}}(\boldsymbol{\theta}) = \sum_{j=1}^{M} \hat{u}_N^{\mathrm{LF},j}(\boldsymbol{\theta})\ \hat{u}_N^{\mathrm{AC},j}(\boldsymbol{\theta}), \tag{9}$$

where $\hat{u}_N^{\mathrm{AC},j}(\boldsymbol{\theta})$ is the gPCE of the j-th additive correction (AC) factor (i.e. the difference between the j-th less refined structural model and the high-fidelity one). It is possible to prove that if the number of samples used to train the gPCE of the various model classes tends to infinite, then Equation 9 tends to the solution of the HF model [35].

Equation 9 is then transposed at the gPCE coefficient level through the optimal weight recombination method,

$$\boldsymbol{b}^{\mathrm{MF}} = \sum_{j=1}^{M} \boldsymbol{b}_j^{\mathrm{LF}} + \boldsymbol{w}_j \circ \left(\boldsymbol{b}^{\mathrm{HF}} - \boldsymbol{b}_j^{\mathrm{LF}}\right). \tag{10}$$

In Equation 10, $\circ$ is the Hadamard product (i.e. the element-wise multiplication), while $\boldsymbol{b}^{\mathrm{MF}}$, $\boldsymbol{b}^{\mathrm{HF}}$ and $\boldsymbol{b}_j^{\mathrm{LF}}$ are the gPCE coefficient vectors of the multi-fidelity, the high-fidelity and the j-th low-fidelity model, respectively. $\boldsymbol{w}_j \in$

$[0,1]^N$ is the weight vector that is determined through the minimisation of the normalised empirical error ϵ_{emp} [36] calculated over a set of L HF model outputs

$$\epsilon_{emp} = \frac{\sum_{l=1}^{L}\left[u^{\mathrm{HF}}(\boldsymbol{\theta}_l) - \hat{u}_N^{\mathrm{MF}}(\boldsymbol{\theta}_l)\right]^2}{\sum_{l=1}^{L}\left[u^{\mathrm{HF}}(\boldsymbol{\theta}_l) - \hat{\mu}_{\mathrm{HF}}\right]^2}. \tag{11}$$

In Equation 11, $\hat{\mu}_{\mathrm{HF}} = 1/L \sum_{l=1}^{L} u^{\mathrm{HF}}(\boldsymbol{\theta}_l)$ is the mean of the high-fidelity computational model response for the given set of model outputs. Although ϵ_{emp} may lead to overfitting [36], it is commonly adopted for the construction of multi-fidelity models [35] because it is computationally inexpensive. In addition, defining the multi-fidelity surrogate model at the gPCE coefficient level through Equations 10 and 11 leads to a procedure that does not require using the same sample paths for different numerical models.

The IM variability is inherently considered in the seismic fragility derivation and according to the method adopted in every specific case. For instance, in the cloud-based approach for non-linear demand and fragility estimation (the one adopted in this paper), the IM variability is modelled using a set of unscaled ground-motion records for the EDP estimation and the fragility parameter derivation. Therefore, the IM variability contributes to the variability of the fragility model parameters.

Sample space partitioning and adaptive sampling

The proposed gPCE-MFRF approach can be effective only if combined with an analysis strategy aimed at minimising the total computational cost of the fragility derivation. In other words, the proposed framework is beneficial only if the required accuracy in the resulting fragility model can be achieved with a computational effort lower than that required by the use of the HF model only.

Since the gPCE-MFRF does not require either the solutions of the HF and LF models to be calculated for the same samples or the sample paths of different model classes to have the same size (Equation 10), an analysis strategy can be defined in terms of sampling approach. Particularly, the sampling rule defined in this Section controls how frequently and for which set of random variables any particular LF model is analysed with respect to the HF one.

For instance, the HF and the LF models may be analysed with the same proportion (i.e. same number of analyses) and for the same parameter sets. Although this is the simplest way to apply the method proposed in this paper, it does not lead to any benefits from the computational perspective. Given a target accuracy for the resulting fragility model, an optimal sampling approach would require the optimisation of the total computational cost balancing the burden related to each model class. This clearly depends on the problem under investigation, but as a general and intuitive rule, the optimisation of the computational cost can be defined by introducing ratios (K_i) between the number of analyses of the HF model and those of the LF ones. That is, for instance, $K_i = 1/4$ means that for every single analysis of the HF model, the i-th LF one is analysed four times. An ad-hoc sampling rule is then needed to improve the performance of the proposed approach further. In fact, having different K_i means that each model is characterised by a different number of analyses for every single reference HF analysis (this derives directly from the definition of K_i). In this study, the following strategy is adopted.

Once a parameter set ($\boldsymbol{\theta}^*$) is sampled from the parameter distributions, it is associated with the HF model, i.e. it represents the point in the space of the random variables for which the HF model is analysed. Then, for every single i-th LF model class, N_i (i.e. $N_i = 1/K_i$) new parameter sets are sampled according to a proposal distribution centred on the actual point ($\boldsymbol{\theta}^*$), that is $q_{\mathrm{local}}(\boldsymbol{\theta}_k^*|\boldsymbol{\theta}^*)$, where $k = [1, N_i]$. The calibration of $q_{\mathrm{local}}(\boldsymbol{\theta}_k^*|\boldsymbol{\theta}^*)$ allows an analyst to manage the distances between the LF samples and the HF one. The factors K_i are unknown a priori, but they could be tuned to minimise the total computational cost. The calibration of the optimal K_i is out of the scope of the present paper, but it represents one of the focuses of future studies. In the case study presented in the next Section, the results of a sensitivity analysis on the value of K_i are reported to provide readers with practical considerations.

In the calculation of structural fragility, the region of the probability space close to the limit state related to the DS under investigation is the primary concern, i.e. where most of the probability (of failure) mass is concentrated and where the solutions of LF models may differ from those of the HF one. Therefore, the computational strategy proposed in this Section can be further improved by partitioning the probability space in a few regions (three, in this case: *safe*,

failure and *transition* regions), as shown in Figure 2, in which different sets of K_i are defined. The main idea is to have a very accurate multi-fidelity gPCE in the region of the sample space close to the limit state and accept a lower accuracy elsewhere. Each region can be easily defined in terms of $DCR_{DS_i}^{HF}$ of the HF model such that,

$$\begin{aligned}
&\Omega_{\text{Safe}} = \left\{\boldsymbol{\theta} \in \Omega_{\boldsymbol{\theta}}\,, IM | DCR_{DS_i}^{HF}(\boldsymbol{\theta}, IM) < lb_{DS_i}\right\},\\
&\Omega_{\text{Transition}} = \left\{\boldsymbol{\theta} \in \Omega_{\boldsymbol{\theta}}\,, IM | lb_{DS_i} \leq DCR_{DS_i}^{HF}(\boldsymbol{\theta}, IM) \leq ub_{DS_i}\right\},\\
&\Omega_{\text{Failure}} = \left\{\boldsymbol{\theta} \in \Omega_{\boldsymbol{\theta}}\,, IM | DCR_{DS_i}^{HF}(\boldsymbol{\theta}, IM) > ub_{DS_i}\right\}.
\end{aligned} \tag{12}$$

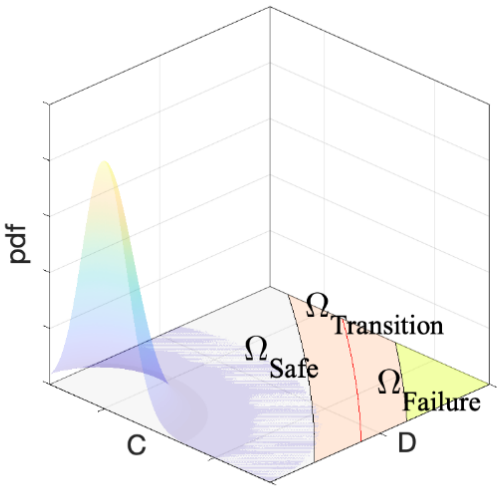

Figure 2 Sample space partitioning.

In the previous Equation, lb_{DS_i} and ub_{DS_i} are lower and upper bounds, respectively. Their definition can be based on either practical considerations or the accuracy of less refined models. This latter strategy is adopted in the present study,

$$\begin{aligned}
lb_{DS_i} &= \min\left\{DCR_{DS_i}^{HF}, DCR_{DS_i}^{LF,1}, \dots, DCR_{DS_i}^{LF,j}, \dots, DCR_{DS_i}^{LF,M}\right\},\\
ub_{DS_i} &= \max\left\{DCR_{DS_i}^{HF}, DCR_{DS_i}^{LF,1}, \dots, DCR_{DS_i}^{LF,j}, \dots, DCR_{DS_i}^{LF,M}\right\}.
\end{aligned} \tag{13}$$

Such a procedure would require knowing a priori the region where a particular sample set $\boldsymbol{\theta}$ lies. This is clearly not possible. However, gPCE-based predictive models of DCR_{DS_i} for every model class can be built without any additional cost ($\widehat{DCR}_{DS_i}^{\text{gPCE}}(\boldsymbol{\theta}, IM)$, Equation 4). In fact, the same samples adopted for the fragility relationship derivation can be used for this purpose. It is worth noting (and intuitive) that the accuracy of the gPCE-based predictive models improves as the number of samples used for its calibration increases.

The structure of the computational approach proposed so far is suitable for being used in conjunction with an adaptive sampling strategy [37]. The gPCE-based predictive models of DCR_{DS_i}, adopted to determine the region where a particular $\boldsymbol{\theta}$ lies, can be also used to optimise the sampling path. The Kullback–Leibler divergence ($D_{KL}(\cdot)$) [16] is a natural choice when Bayesian inference is involved [38]. In the context of the Bayesian inference, the Kullback–Leibler divergence can be thought of as a measure of the information gained by updating a prior distribution $f(\boldsymbol{\chi}_{\text{MFRF}})$ to the posterior one $f\left(\boldsymbol{\chi}_{\text{MFRF}}|\mathbf{y}(\boldsymbol{\theta})\right)$, that is

$$D_{KL}\left(f\left(\boldsymbol{\chi}_{\text{MFRF}}|\mathbf{y}(\boldsymbol{\theta})\right)||f(\boldsymbol{\chi}_{\text{MFRF}})\right) = \int_{\Omega_{\boldsymbol{\theta}}} f\left(\boldsymbol{\chi}_{\text{MFRF}}|\mathbf{y}(\boldsymbol{\theta})\right) \ln\left[\frac{f(\boldsymbol{\chi}_{\text{MFRF}}|\mathbf{y}(\boldsymbol{\theta}))}{f(\boldsymbol{\chi}_{\text{MFRF}})}\right] d\boldsymbol{\theta}. \tag{14}$$

For the sake of clarity, it is important to emphasise again that the vector of the analysis result $\mathbf{y} = \left(DCR_{DS_i}^{HF}(\boldsymbol{\theta}), DCR_{DS_i}^{LF,1}(\boldsymbol{\theta}), \dots, DCR_{DS_i}^{LF,j}(\boldsymbol{\theta}), \dots, DCR_{DS_i}^{LF,M}(\boldsymbol{\theta})\right)^{\text{T}}$ is a function of the model parameter vector $\boldsymbol{\theta}$. Let us consider a second global proposal distribution $q_{\text{global}}(\boldsymbol{\theta}_m^*|\boldsymbol{\theta}^*)$ generating M_{cand} parameter sets $\boldsymbol{\theta}_m^*$ which are potential

candidates for a new step in the adaptive sampling procedure. The one which maximises the Kullback–Leibler divergence ($\overline{\boldsymbol{\theta}}$) is also the parameter set leading to the maximum information gain. Once the parameter set $\overline{\boldsymbol{\theta}}$ is selected, $q_{\text{local}}(\boldsymbol{\theta}_k^*|\boldsymbol{\theta}^*)$ is centred on the selected new step, and the parameter sets for the LF model classes are generated. The proposed procedure is finally summarised in Algorithm 1.

Algorithm 1. Adaptive sampling

1. procedure $(N_{step}, IM, M_{\text{cand.}}, q_{\text{local}}(\cdot\,|\,\cdot), q_{\text{global}}(\cdot\,|\,\cdot), \Omega_{\boldsymbol{\theta}})$

2. for $i = 1$ to N_{step} **do**

3. sample M_{cand} candidates $\boldsymbol{\theta}_m^*$ according to $q_{\text{global}}(\boldsymbol{\theta}_m^*|\boldsymbol{\theta}_i)$

4. predict the region of $\Omega_{\boldsymbol{\theta}}$ where each $\boldsymbol{\theta}_m^*$ lies through the use of $\widehat{DCR}_{DS_i}^{\text{gPCE,HF}}(\boldsymbol{\theta}_m^*, IM)$ (HF surrogate model based on the gPCE)

5. for each i-th model class, use $q_{\text{local}}\left(\boldsymbol{\theta}_{m,K_i}^*|\boldsymbol{\theta}_m^*\right)$ to sample $1/K_i$ points $\boldsymbol{\theta}_{m,K_i}^*$ for each $\boldsymbol{\theta}_m^*$ (K_i is selected according to the region where each $\boldsymbol{\theta}_m^*$ sample is located)

6. calculate $\widehat{DCR}_{DS_i}^{\text{gPCE,LF}_i}\left(\boldsymbol{\theta}_{m,K_i}^*, IM\right)$ of less refined model classes, where $\widehat{DCR}_{DS_i}^{\text{gPCE,LF}_i}\left(\boldsymbol{\theta}_{m,K_i}^*, IM\right)$ is the gPCE-based surrogate model of the LF_i model classes

7. use the surrogate models, $\widehat{DCR}_{DS_i}^{\text{gPCE,HF}}(\boldsymbol{\theta}_m^*, IM)$ and $\widehat{DCR}_{DS_i}^{\text{gPCE,LF}_i}\left(\boldsymbol{\theta}_{m,K_i}^*, IM\right)$, to calculate $p\left(\boldsymbol{\chi}_{\text{MFRF}}|\hat{\mathbf{y}}(\boldsymbol{\theta}_m^*)\right)$ for each set of solutions $\hat{\mathbf{y}}(\boldsymbol{\theta}_m^*)$ related to $\boldsymbol{\theta}_m^*$ and $\boldsymbol{\theta}_{m,K_i}^*$

8. calculate $D_{KL}\left(f\left(\boldsymbol{\chi}_{\text{MFRF}}|\hat{\mathbf{y}}(\boldsymbol{\theta}_m^*)\right)||f(\boldsymbol{\chi}_{\text{MFRF}})\right)$ for each set of solutions $\hat{\mathbf{y}}(\boldsymbol{\theta}_m^*)$ related to $\boldsymbol{\theta}_m^*$ and $\boldsymbol{\theta}_{m,K_i}^*$

9. select $\overline{\boldsymbol{\theta}}_m^*$ such that $\max_{\overline{\boldsymbol{\theta}}_m^*} D_{KL}\left(f\left(\boldsymbol{\chi}_{\text{MFRF}}|\hat{\mathbf{y}}(\boldsymbol{\theta}_m^*)\right)||f(\boldsymbol{\chi}_{\text{MFRF}})\right)$

10. solve HF considering $\overline{\boldsymbol{\theta}}_m^*$ and LF considering $\overline{\boldsymbol{\theta}}_{m,K_i}^*$, $DCR_{DS_i}^{\text{HF}}(\overline{\boldsymbol{\theta}}_m^*, IM)$ and $DCR_{DS_i}^{\text{LF}_i}\left(\overline{\boldsymbol{\theta}}_{m,K_i}^*, IM\right)$ respectively. Analysis results of the structural models $DCR_{DS_i}^{\text{HF}}(\overline{\boldsymbol{\theta}}_m^*, IM)$ and $DCR_{DS_i}^{\text{LF}_i}\left(\overline{\boldsymbol{\theta}}_{m,K_i}^*, IM\right)$ are collected in $\mathbf{y}(\overline{\boldsymbol{\theta}}_m^*)$

11 use solutions calculated at the previous step $\mathbf{y}(\overline{\boldsymbol{\theta}}_m^*)$ to update the gPCE-based surrogate models, $\widehat{DCR}_{DS_i}^{\text{gPCE,HF}}$ and $\widehat{DCR}_{DS_i}^{\text{gPCE,LF}_i}$

12. calculate $f\left(\boldsymbol{\chi}_{\text{MFRF}}|\mathbf{y}(\overline{\boldsymbol{\theta}}_m^*)\right)$

13. set $\boldsymbol{\theta}_{i+1} = \overline{\boldsymbol{\theta}}_m^*$ and $f(\boldsymbol{\chi}_{\text{MFRF}}) = f\left(\boldsymbol{\chi}_{\text{MFRF}}|\mathbf{y}(\overline{\boldsymbol{\theta}}_m^*)\right)$

14. end for

15. end procedure

It is finally worth noting that the computational cost of the adaptive importance sampling algorithm is negligible compared to the computational cost of the HF model.

Procedure calibration

The gPCE-MFRF method for fragility derivation and the adaptive sampling approach proposed in this paper requires an appropriate calibration process to be effective in practice.

The gPCE of a random variable always requires setting some key parameters, and the method discussed here is not an exception. Specifically, the polynomial expansion cardinality (N), the families for the orthogonal basis functions ($\psi_{\mathbf{i}}$), and the number of analyses, must be set to build an expansion that meets the target accuracy.

The polynomial expansion cardinality (N) has to be chosen by pursuing the accuracy of the surrogate model while avoiding potential overfitting issues [39]. There is no specific rule that can drive an analyst towards an *a-priori* choice of the optimal gPCE cardinality, as this depends on the shape of the problem under investigation. However, a few preliminary analyses are usually sufficient to empirically assess the impact of N on the surrogate model and then to select the most appropriate value.

The families of polynomial functions (ψ_i), to be used as the basis for the gPCE, are chosen according to the PDF of the random variables collected in $\boldsymbol{\theta}$. Readers may refer to Xiu [40] for a more comprehensive discussion on this topic.

The number of analyses must be decided by balancing the required target accuracy for the surrogate model and the available computational performance. An error metric is generally selected in practical applications and monitored until the surrogate model accuracy reaches a prefixed target. The empirical error ϵ_{emp} minimised in Equation 11 for the derivation of the gPCE coefficients of the multi-fidelity surrogate model can also be tracked, and analyses can be added until it reaches the target accuracy.

For the sake of simplicity, the calibration of a gPCE is presented in this Section as a chain of decisions. The calibration step should be seen as a comprehensive process in which the three points discussed above are addressed together. Setting the ratios K_i, between the number of analyses for different model classes, as well as the parameters defining the sample space partitioning, would imply the solution of a high-dimensional optimisation problem. Alternatively, empirical strategies can be employed to calibrate these parameters. Given the average analysis durations for each model class, one could calibrate K_i to minimise the computational cost, assuming it is described through a time metric.

The sample space partitioning can be based on either practical consideration or the accuracy of less refined models. In the former case, an analyst may already know the problem under investigation and then make a reliable prediction on the position and shape of the limit state surface. If this is not possible, one can assume that the edges of the transition region are defined by the envelope of the limit state surfaces related to different model classes. The logic describing this latter condition, adopted in this paper, is reported in Equation 13. As previously mentioned, gPCE-based surrogate models of DCR_{DS_i} for each model class can be built without any additional cost to forecast where a sample set $\boldsymbol{\theta}$ will lay.

Being based on gPCEs of fragility model parameters, the proposed gPCE-MFRF, as well as the adaptive sampling, remain unchanged while the number of random variables in $\boldsymbol{\theta}$ increases or decreases. On the other hand, increasing the size of $\boldsymbol{\theta}$ leads to a higher number of orthogonal basis functions and (potentially) a larger number of analyses required to reach a target accuracy of the surrogate model. Regarding this latter point, the number of additional analyses required for each new uncertain parameter in $\boldsymbol{\theta}$ depends on its variability (as expected), interaction with the other random variables (e.g. conditionality), and the shape of the model response varying that specific parameter (e.g. linear, non-linear).

CASE-STUDY APPLICATION

Building description

An archetype RC building, representative of school buildings in Southeast Asia (e.g. Philippines, Indonesia), and defined based on a data collection involving rapid visual surveys for over 200 school buildings [41,42], is analysed in this Section to test the feasibility of the proposed procedure. A statistical analysis of the geometry data collected during the surveys (Figure 3a-f) shows that such school buildings somehow comply with a local "design template". Therefore, the surveyed sample is remarkably homogeneous. The parameters related to the longitudinal direction of the building are characterised by a higher variability than those associated with the transverse direction (e.g. 90% of the buildings in the survey have three transverse bays). As shown in Figure 3a-f, the number of longitudinal bays ($N_{bays,x}$) is the most variable geometrical parameter. Other features such as the number of storeys, length of the transverse bays, dimension of the beams/columns show negligible variability within the surveyed sample. Therefore, the analysed structure is a two-storey rectangular-plan RC frame (Figure 4a) representing the longitudinal frame of the archetype building. Consistently with the assumptions in Gentile and Galasso [5], the uncertain parameters $\boldsymbol{\theta}$ selected for this application are the number of longitudinal bays of the frame, the concrete compressive strength, and the steel yield stress. These last two parameters, which highly influence the capacity and failure mechanism of the frame members, are considered random since they are not directly investigated in the survey.

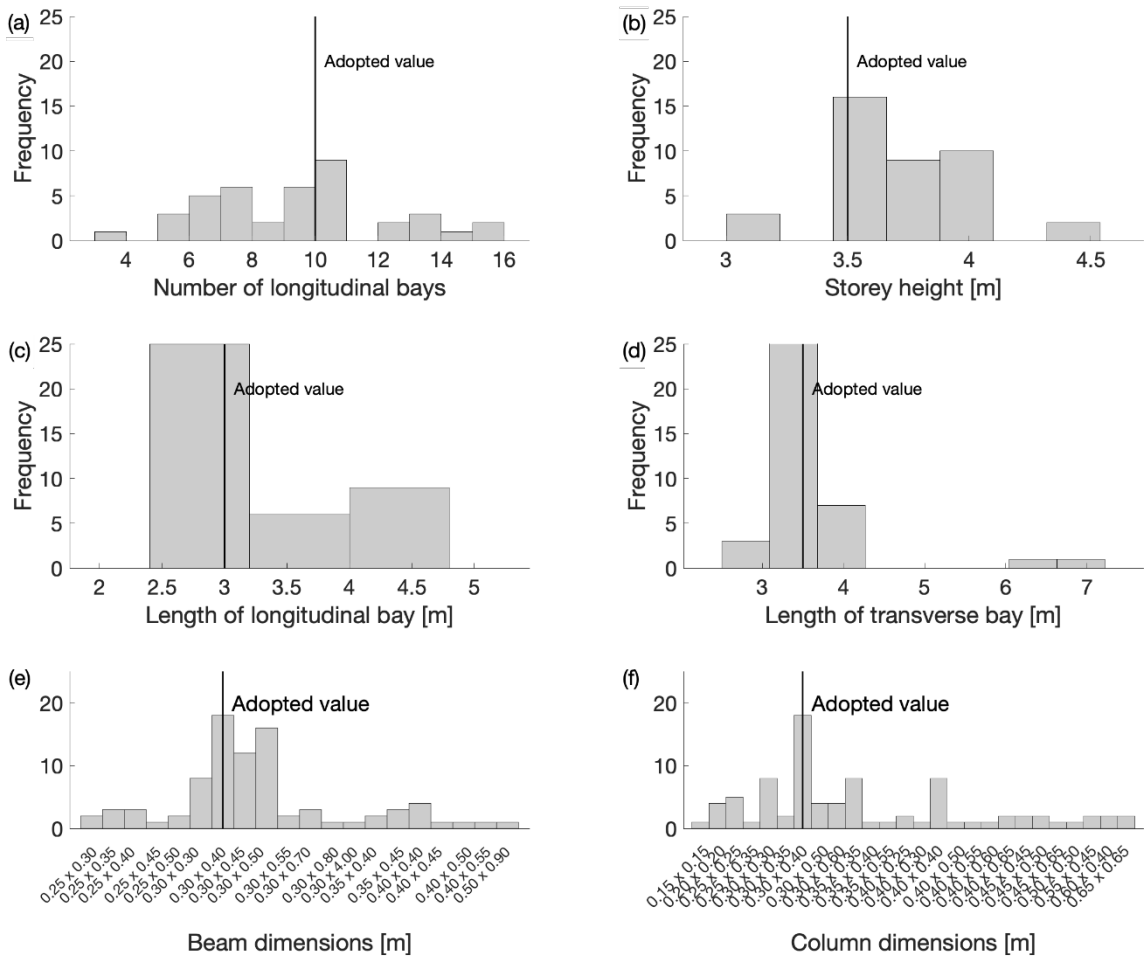

Figure 3 Geometry trends and adopted values defining the archetype RC frame. Modified after Gentile et al., 2019.

Specifically, since the data collection is based on a rapid visual survey, the empirical distribution of the number of longitudinal bays is available (Figure 4b). In contrast, no direct information about the material properties is accessible. According to Southeast Asian statistics (e.g. [43]), the concrete cylindrical compressive strength (f_c) and steel yield stress (f_y) in the region have average values of 24MPa and 400MPa, respectively. Coefficients of variation (CoV) values equal to 18% and 5% for the concrete cylindrical strength and steel yield stress, respectively, can be found in the scientific literature (e.g. [44]). Based on these values, lognormal distributions are defined for f_c and f_y. Since the schools comply with a template design, the same nominal value of material properties is considered for all the buildings in the considered portfolio. Hence, the building-to-building variability in material properties coincides with their within-building variability.

It is worth mentioning that the values of f_c and f_y have a direct effect on the characterisation of the RC beams, columns and joint panels; in particular:

- Moment-curvature analysis (including gravity axial load) is used to calculate the flexural capacity of beams and columns. The model by Mander [45] is used for concrete, including the calculation of its confined ultimate strain (ε_{cu}). Concrete modulus of elasticity is equal to $5000\sqrt{f_c}$,. The model by King [46] is used for steel. In particular, the ultimate steel stress is equal to $1.3f_y$;
- The model by Priestley and Park [47] is used to calculate the equivalent plastic hinge length, which linearly depends on f_y;

- The beam/column drift related to bar buckling depends on both f_c and f_y, since it is calculated according to the deformation-based model by [48]);
- The shear capacity of beams and columns depends on both f_c and f_y, since it is calculated according to [49];
- The joint shear stress capacity is calculated using Mohr's circle approach. The joint stress is attained its principal/compressive stress capacity is achieved (proportional to $\sqrt{f_c}$).

This approach neglects the experimental-vs-theoretical modelling uncertainty of the parameters derived using the above-mentioned empirical models. Although this simplified assumption is deemed reasonable to illustrate the proposed procedure, more refined applications should include this effect, for example, by simulating experimental-vs-theoretical ratios for each random model parameter. Moreover, the adopted simplified assumptions imply a perfect correlation between some parameters (e.g. concrete compressive strength and elastic modulus). It is advisable to explicitly consider such correlation in more advanced applications, including spatial correlation of the considered random variables. A more advanced procedure to include modelling uncertainties in seismic response analyses is provided in [3], among others.

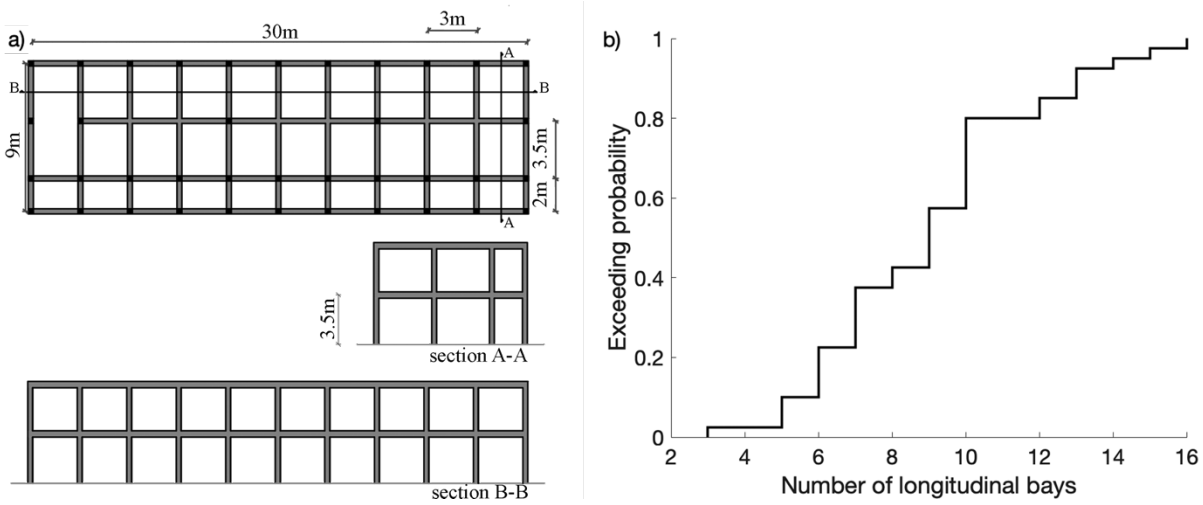

Figure 4 Archetype RC frame: a) structure under investigation; b) empirical distribution of the number of longitudinal bays. Modified after [5]**.**

Structural detailing is critical to define the numerical models for the fragility calculation. Therefore, the archetype building is simulated-designed according to the Uniform Building Code 1994 [50] and the American Society of Civil Engineers (ASCE 7-10, 2017) [49]. The use of these building codes is justified because most Southeast Asia countries have adopted seismic provisions consistent with them [25,52]. In particular, a low code target design, consistently with the HAZUS MH4, HAZard United States [53], is considered. The resulting detailing features are reported in Table 1.

It is worth stressing that choosing a simple case study (as the one selected here) allows focusing the discussion on the proposed procedure rather than on the details of the specific structural model. However, this choice is not deemed to jeopardise the generality of the proposed approach.

Table 1 Structural detailing of the archetype building.

	Typical beam	Typical column	Typical joint
Low Code	30x40cm 3 ϕ 16 top (ρ_l=0.5%) 3 ϕ 16 bottom (ρ_l=0.5%) ϕ 10@150mm stirrups (ρ_t=0.65%)	30x40cm 8 ϕ 16 perimeter (ρ_l=1.3%) ϕ 10@100mm stirrups (ρ_t=1.0%)	No stirrups

Model classes

Two model classes varying in refinement are adopted in this study. The lowest-refinement model class is based on SLaMA [25,54]. This method allows plastic mechanisms and capacity curve (i.e. a force-displacement curve) of RC frames, wall and dual-system buildings to be estimated employing a "by-hand" procedure (i.e. through an electronic spreadsheet). SLaMA is based on the calculation of the hierarchy of strength at sub-system level. The local results are then combined by adopting equilibrium and compatibility principles to obtain the global capacity curve. In addition, many failure mechanisms (i.e. flexure, bar buckling, lap-splice failure, shear) are considered for each member of the system. In this way, the weakest link drives the overall structural behaviour.

Non-linear time-history analyses (NLTHAs) performed on a refined, two-dimensional numerical model represent the highest model class. The adopted modelling strategy, previously validated on experimental results, is based on a lumped plasticity approach and is summarised in Figure 5. The revised Takeda hysteretic model [55] is adopted for beams and columns, with the columns having a thinner loop. The hysteretic behaviour of the beam-column joints is modelled using the Modified Sina model [55], which can capture their pinching phenomenon. More details on the adopted modelling assumptions are given in [56].

For both model classes, the same set of analytical models are used to characterise beams, columns and joint panels according to their possible failure mechanisms (i.e. flexure, shear, bar buckling, lap-splice failure. Such models, described in detail in [56], are explicitly dependent on the variability of the concrete compressive strength and the steel yield stress.

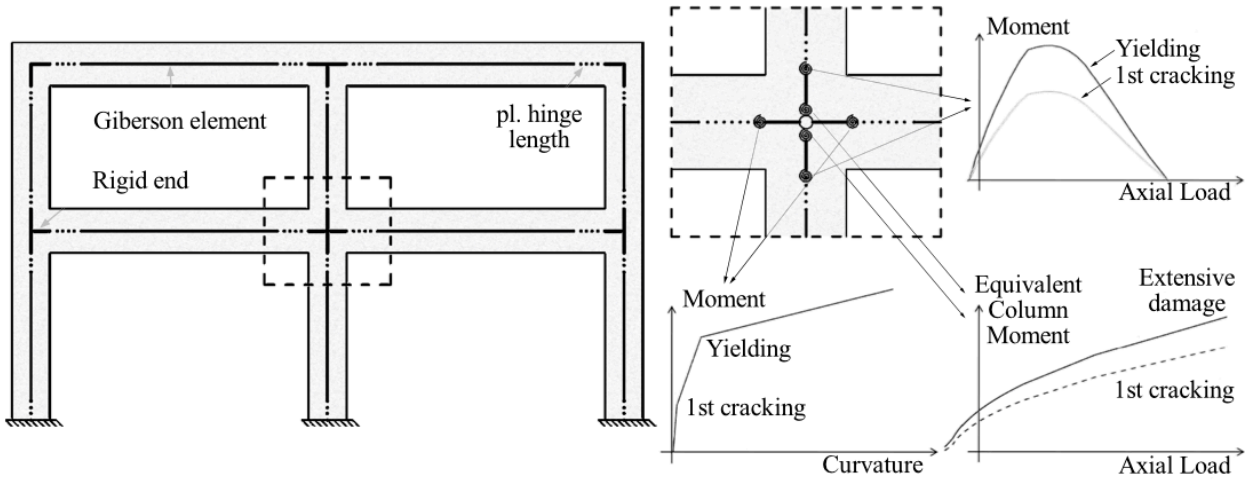

Figure 5 Lumped plasticity-based numerical modelling strategy [25]**. Beams follow a tri-linear Moment-Curvature law. Columns are characterised according to their Moment-Axial load diagram. Joints follow the Equivalent Column Moment-Axial load diagram. Flexure, shear, bar buckling and lap-splice failure mechanisms of the members are explicitly considered.**

A cloud analysis (Jalayer et al. 2015) is used to compute EDP estimates for a set of ground-motion records. This can be directly applied in the case of NLTHAs (the highest refinement level). In contrast, for the low refinement model class, the capacity spectrum method [57] is adopted according to the assumptions described in Gentile and Galasso, 2020a.

A set of 150 ground motion records is considered in this study, which is regarded as a statistically significant number in relation to fragility analysis. They are a subset of the *Selected Input Motions for displacement-Based Assessment and Design* (SIMBAD, [58]) database, which includes 467 tri-axial accelerograms, generated by 130 worldwide seismic events (shallow crustal earthquakes with moment magnitudes ranging from 5 to 7.3 and epicentral distances up to 35 km). The selected ground motion records are arbitrarily chosen by ranking the entire database in terms of peak ground acceleration (PGA) values (by using the geometric mean of the two horizontal components) and then keeping the component with the largest PGA value (for the 150 stations with highest mean PGA). Such selection is

compatible with the cloud-based approach, which does not require a site-specific, hazard-consistent record selection, and it requires none-to-moderate scaling of the ground motions.

Fragility relationships are derived considering the maximum inter-storey drift as the EDP of interest and the average spectral acceleration (Avg S_a) as an IM. Avg S_a is defined as the geometric mean of spectral-acceleration values in the range of period ($T_{1,min}$: 1.5 $T_{1,max}$), where $T_{1,min} = 0.38\ s$ is the minimum first-mode period (considering the entire database of building samples generated varying $N_{bays,x}$, f_c and f_y) while $T_{1,max} = 0.53\ s$ is the maximum one. Four structure-specific DSs (Slight Damage, Moderate Damage, Extensive Damage, Complete Damage), which are based on the HAZUS definitions, are investigated in this study. Such DSs are quantified based on the actual pushover curve of the consider building samples Figure 6a shows the capacity curve of the building sample with average values for $N_{bays,x}$, f_c and f_y, together with the calculated plastic mechanism at DS3 (Figure 6b). The corresponding drift limits, [0.25, 0.6, 1.5, 2] %, are assumed as representative of the entire building class.

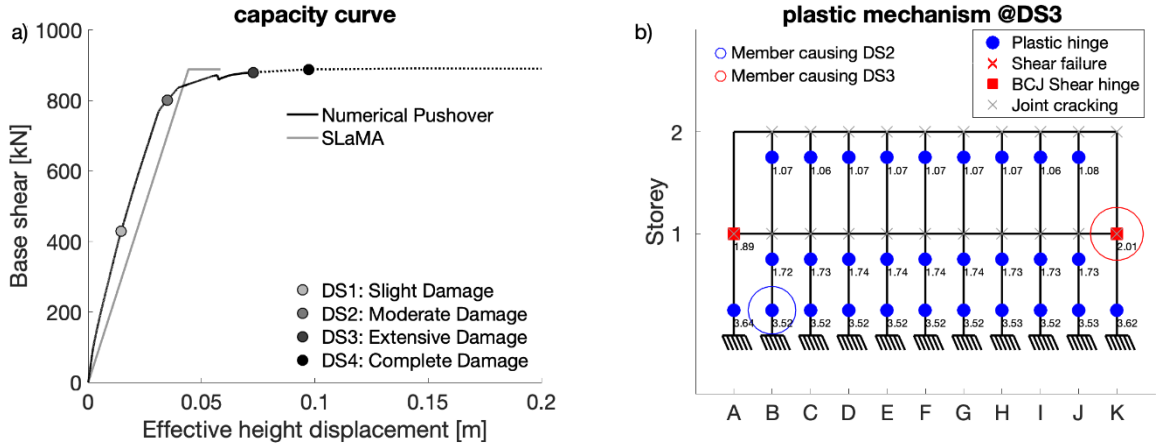

Figure 6 a) non-linear static capacity curves; b) plastic mechanism at DS3. Modified after Gentile, et al., 2019.

Results and discussion

In this Section, the feasibility of the proposed method is demonstrated by comparing gPCE-MFRF-based fragility relationships with those obtained following other approaches. Specifically, fragility relationships explicitly fitted on HF model results, through the maximum likelihood estimation [59] (labelled as "MLE" fragility relationships in the following), are assumed as a reference solution for benchmarking purposes. The benchmark case uses 15,000 samples, i.e. 150 ground motions (described above) and 100 realisations of the vector $\boldsymbol{\theta}$ (i.e. model parameters). The proposed method is applied considering four different cases: 1) using only HF model results (labelled as "gPCE-HFRF"); 2) deriving MF model with $K_1 = 1$ (labelled as "gPCE-MFRF k1"); 3) deriving MF model with $K_2 = 0.5$ (labelled as "gPCE-MFRF k2"); 4) deriving MF model with $K_3 = 0.25$ (labelled as "gPCE-MFRF k3"). These three different assumptions on the K_i value allows for a comprehensive understanding of the role played by this parameter in the proposed approach.

As discussed above, the construction of the multi-fidelity gPCE of the fragility parameters in $\boldsymbol{\chi}_{\mathrm{MFRF}}$ requires the basis function family and the polynomial expansion degree to be specified. The basis polynomial functions ($\psi_{\mathbf{i}}$) are chosen according to the PDF of the random variables collected in $\boldsymbol{\theta}$ [15]. Assuming that the f_c and f_y are log-normally distributed, and that $N_{bays,x}$ follows an empirical distribution (as discussed above), Hermitian polynomials are used as basis functions [15]. As discussed above, no specific rule can drive an *a-priori* choice of the optimal gPCE cardinality, as this depends on the shape of the problem under investigation. However, a few preliminary analyses are usually sufficient to empirically assess the impact of N on the surrogate model and select the most appropriate value.

The optimal polynomial expansion degrees are then selected based on the results of preliminary sensitivity analysis (not reported here for brevity), in which the normalized empirical error ϵ_{emp} was used to compare different

assumptions. In particular, 4-*th* order polynomial expansions are used for the parameters related to the high-fidelity model, while 3-*th* order polynomial expansions are adopted for those related to the lowest refinement level. More details about the calibration of a gPCE can be found in the dedicated Section above.

Once the structure of the multi-fidelity gPCE is defined, fragility relationships are derived for each different strategy (i.e. MLE, gPCE-HFMF, gPCE-MFHF), varying the number of samples. Finally, the resulting fragility model parameters are used to calculate relative errors with respect to the final MLE results (with 15,000 samples). The relative errors versus sample numbers for the median and standard deviation of the fragility model (Equation 3) are shown in Figure 7a-d. It is worth noting that the sensitivity analysis results for the other parameters and/or for other DS are consistent with those in Figure 7a-d. In addition, DS3 and DS4 are the damage states for which fragility relationships show the highest variability.

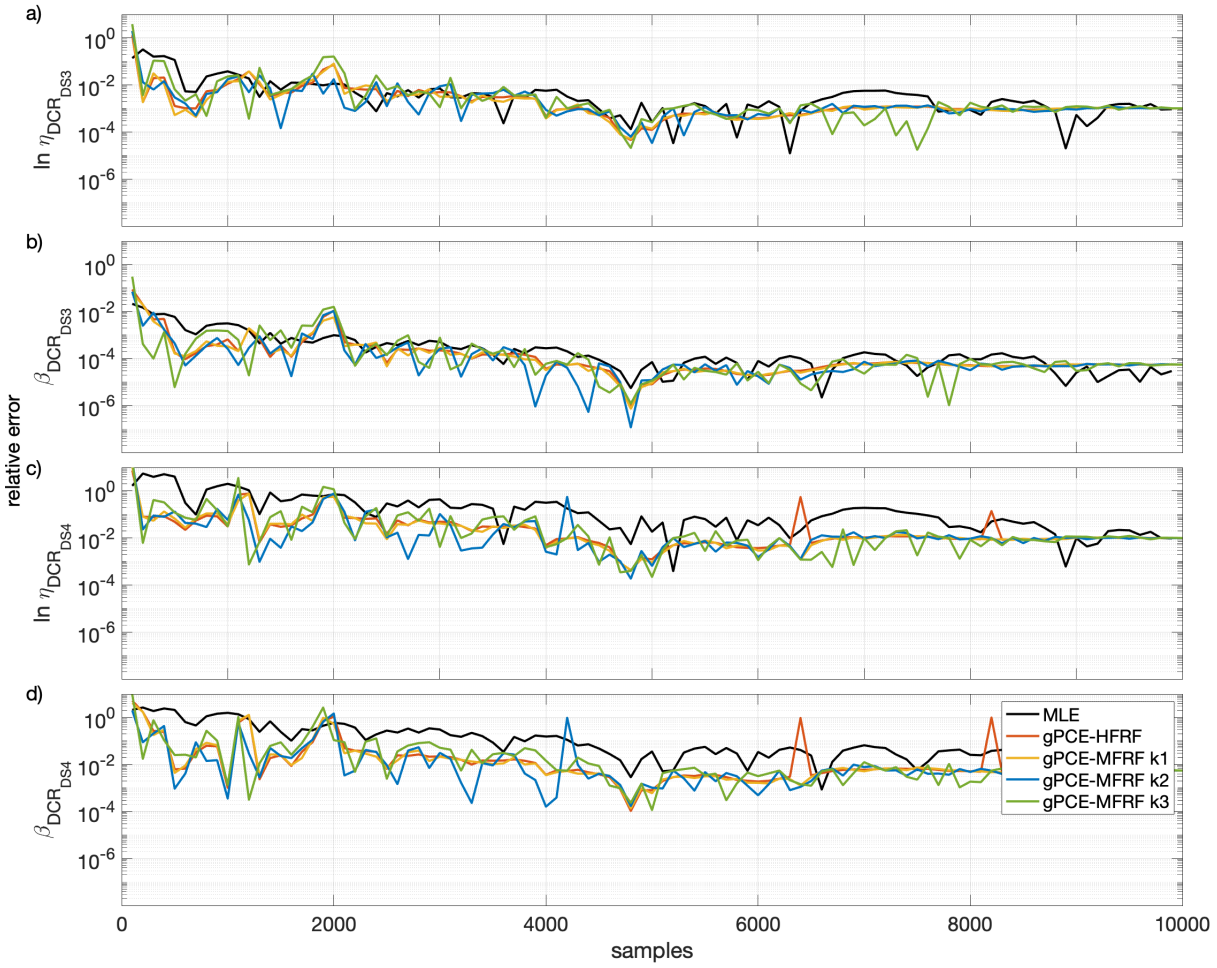

Figure 7 Relative errors: a) DS3 - $\ln\eta_{DS_3}$; b) DS3 - β_{DS_3}; c) DS4 - $\ln\eta_{DS_4}$; d) DS4 - β_{DS_4}.

The errors of the different approaches show the same trend, even though the proposed approach performs slightly better in all four cases. Varying K_i does not affect the error trend. However, the reduction of K_i leads to higher local variability of the error, which seems less stable than in the case of higher K_i. In fact, for a high value of K_i, most of the terms of the weight vector $\boldsymbol{w}_j$ (Equation 10) are equal (or close) to 1, which means that the coefficients $\boldsymbol{b}^{\mathrm{MF}}$ are very close to $\boldsymbol{b}^{\mathrm{HF}}$. On the other hand, when K_i decreases, the values of $\boldsymbol{w}_j$ show higher variability in the range $[0,1]^N$, thus justifying such higher oscillation of the error.

Given a particular number of samples, Figure 7 does not show a clear difference in the errors of "gPCE-HF" and "gPCE-MF", which would justify the use of different model classes. This is mainly due to two reasons. Firstly, the simple case study which converges to a stable error after a few thousand steps. Secondly, in this sensitivity analysis,

once a K_i is selected, it is also kept fixed in all the sample space. As discussed in the previous Sections, an adaptive algorithm based on the sample space partitioning can improve the method's performance.

An attractive property of the gPCE is the possibility to perform a variance-based sensitivity analysis (i.e. calculation of the Sobol' indices) without any additional computational cost. Such a result provides valuable information to contain the effects of uncertainties on the fragility relationship calculation [9] and derive insights about the system behaviour. Figure 8 shows the first-order Sobol' indices for the HF model under investigation varying IM. For low values of IM, the most affecting parameter is the compressive strength of the concrete f_c. Under low-IM ground motions, the variability of the compressive strength plays a key role. Under this condition, the dynamic behaviour of the structure is controlled by its stiffness, whose variation, given a fixed geometry of the structural members, is entirely driven by the value of f_c through the functional relationships described in the previous sections. In addition, columns are mainly loaded in compression by vertical actions. The shape of the failure domain in that region is determined by the material's compressive strength only, as the geometry of the structural member is fixed. As IM increases, the role played by the variability of different parameters tends to be equal, even though the tensile strength one is slightly higher than the others. In fact, ground motions characterised by high IM values always result in collapses independently of the mechanical characteristics of the structure (for the considered distributions). The Sobol' indices do not show the range in which the model output varies or the effect of a random variable on the model output. They instead show how each random variable, or set of them, affects the variability of the results.

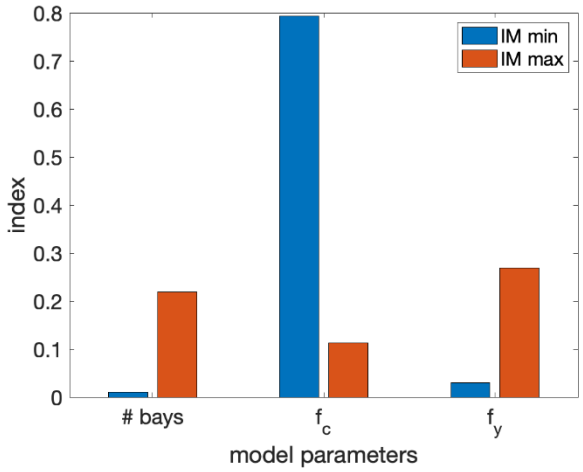

Figure 8 First-order Sobol' indices.

On the basis of the sensitivity analysis results, fragility relationships (Figure 9a-d) are calculated considering: 1) MLE with the complete set of analysis; 2) RF with 7500 samples; 3) gPCE-HFRF with 7500 samples; 4) gPCE-MFRF k2 with 4500 samples; 5) gPCE-MFRF with adaptive sampling (labelled as AS gPCE-MFRF in the following). The number of samples for the fragility derivation in the cases of RF, gPCE-HFRF and gPCE-MFRF k2 is determined considering a target error for the conditional median of DS4 with an order of magnitude in the range of $[10^{-1}, 10^{-2}]$. The adaptive sampling algorithm is used in this application, assuming that the sample space is partitioned into three parts, as previously described. Particularly, $K = 1$ is used in the transition region, while $K = 0.5$ is adopted in the safety and failure regions. The same parameter distributions are also adopted as both local and global proposed distributions.

The fragility relationships derived with the proposed multi-fidelity approach are very close to those calculated with conventional methods (i.e. MLE, RF) for the case of DS1 and DS2. The mean multi-fidelity fragility relationships are fully contained within the confidence interval of the high-fidelity one. In the case of DS3 and DS4, the differences between the proposed approach and existing methods slightly increase. These differences are particularly evident for high values of IM. However, also in the case of DS3 and DS4, the average multi-fidelity fragility relationships are contained within the confidence interval of the high-fidelity one. This indicates that the epistemic uncertainties affect the final result more than the approach adopted for fragility curve derivation. In Table 2, differences among the methods are quantified through the relative error with respect to the MLE results. All the relative errors are close to

the target accuracy required for the final results (e.g. $[10^{-1}, 10^{-2}]$). However, the number of HF analyses strongly decreases from standard methods to the proposed one. Particularly, the proposed adaptive sampling leads to a further reduction of the computational burden, thus highlighting its importance in the feasibility of the proposed approach.

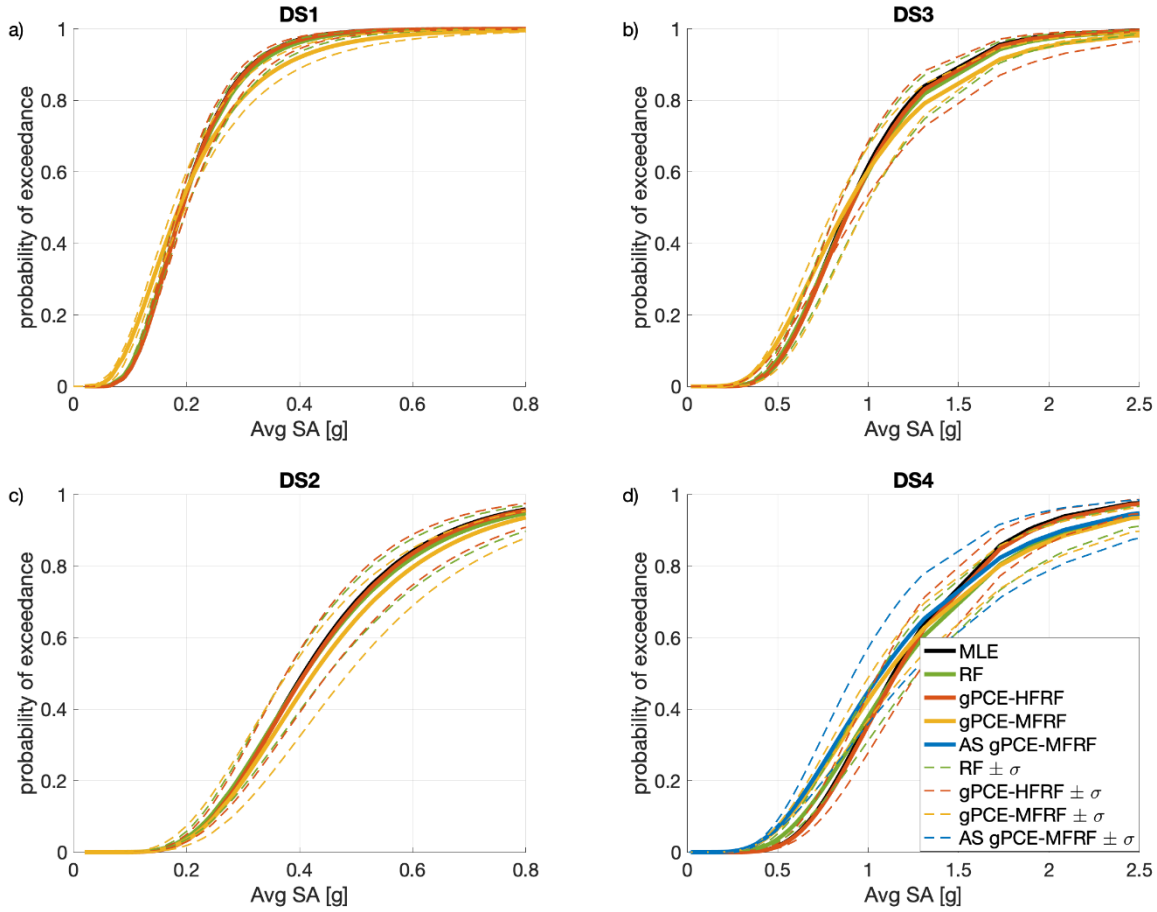

Figure 9 Fragility relationships calculated for different DS: a) DS1; b) DS2; c) DS3; d) DS4.

As mentioned above, the computational burden involved with the LF response analysis method is considerably lower than the HF one. The absolute value of the required computational time may depend on the adopted workstation and the number of analyses running in parallel. For this reason, a relative estimation (HF with respect to LF) is provided here, considering one building sample only. First, both methods require the same time for the mechanical characterisation of every single structural member (approximately 30 seconds for this particular case study). SLaMA then involves calculating the simplified global equilibrium and the execution of the CSM for each ground motion. The time needed for these analytical operations is negligible (less than two seconds, for this case study). On the other hand, approximately 30 seconds are required to run a NLTHA for each of the 150 ground motions (for this case study). This means that the HF-LF computational time ratio ranges between 141 and 151.

Table 2 Summary of the fragility relationship calculation.

Method	HF analyses	LF analyses	Relative error $\ln\eta_{DS_4}$	Relative error β_{DS_4}
MLE	14603 (15000)	0	-	-
LF	0	14603 (15000)	0.0986	0.0474
RF	7500	0	0.0133	0.0251
gPCE-HFRF	7500	0	0.0131	0.0247

gPCE-MFRF (k2)	4500	9000	0.0324	0.0299
gPCE-MFRF (k3.3)	2214	7380	0.0801	0.0433
AS gPCE-MFRF	2214	7532	0.0628	0.0372

The results of the RF and the gPCE-HFRF are very close for every DSs. However, fragility relationships derived from the proposed approach are always characterised by a higher variability. In fact, their confidence intervals are slightly larger than those of the RF curves. This is expected as the use of the LF models, while contributing to reducing the required computational burden for fragility analysis, increase the epistemic uncertainties for a given IM level. It is also important to note that, as expected, the proposed approach leads anyway to errors smaller than those obtained considering LF models only. This latter is the upper bound of the error, which is reduced of about two thirds in case the proposed approach is adopted (i.e. "gPCE-MFRF (k2)"). The gPCE-MFRF is finally adopted considering a number of HF and LF analyses comparable to those adopted in the AS gPCE-MFRF, to further investigate the performance of such an approach. Table 2 shows how the proposed adaptive sampling allows reducing the resulting errors compared to the simple gPCE-MFRF.

As discussed in the previous sections, the number of analyses for each model class should be decided by balancing the computational burden and the required accuracy of the result by optimising a cost function. This fundamental aspect is outside of the scope of this paper. For practical reasons, the number of analyses for each model class is decided a priori based on the results of a sensitivity analysis. The adaptive sampling is the only exception here, as a predefined criterion is used to end the algorithm. Specifically, the algorithm stops if the maximum value of the Kullback–Leibler divergence $\max_{\overline{\boldsymbol{\theta}}_m^*} D_{KL}\left(f\left(\boldsymbol{\chi}_{\mathrm{MFRF}}|\hat{\mathbf{y}}(\boldsymbol{\theta}_m^*)\right)||f\left(\boldsymbol{\chi}_{\mathrm{MFRF}}\right)\right)$ (Algorithm 1) is smaller than a prefixed threshold (i.e. 0.01 in this application) for a number of consecutive steps (i.e. 50 steps in this application).

The proposed approach would result in a higher computational gain if used to derive fragility relationships for more complex structures (e.g. tall buildings, long bridges, dams). In such cases, the simplest possible analysis method is (arguably) a numerical pushover, which may require a much longer computational time with respect to the considered case study. However, assuming that the time required for a NLTHA with a set of ground motions is two orders of magnitude higher than that of a pushover, savings in terms of absolute computational time may be considerable.

Finally, it is worth noting that, although the bias levels of the proposed approach with respect to the full time-history analyses may be non-negligible in some practical applications, their rigorous characterisation allows for their correction. In fact, analysts can use a specific fragility derivation approach, depending on their needs and context, or to calibrate appropriate correction factors for the more simplified methods. Specifically, the obtained results in Table 2 are deemed acceptable for portfolio-level risk assessment exercises or for preliminary, more detailed investigations on single assets.

CONCLUSIONS

The derivation of numerical seismic fragility relationships is a challenging and computationally expensive task when both aleatory and epistemic uncertainties are considered. Several different methods to reduce the computational cost related to fragility derivation can be found in the scientific literature. In this context, particularly powerful is the use of the robust fragility approach in conjunction with cloud analysis.

In this paper, a modification of the robust fragility approach was proposed to enable the use of different model classes in the computation of fragility relationships. The main idea behind the proposed approach is to analyse refined numerical models only when strictly necessary (i.e. when the numerical output is approaching a selected damage state) and use simplified models when the numerical results are far enough from the damage state of interest.

A multi-fidelity general Polynomial Chaos Expansion (gPCE) of the fragility model parameters was proposed to combine different model classes. The Bayesian interpretation of the gPCE coefficient calibration allows one to reduce the computational cost further. In contrast to the classic robust fragility method, the proposed one does not require the use of numerical integration strategies to solve the inverse problem. In fact, conjugated gaussian and approximated Laplace distributions can be successfully adopted to model the gPCE coefficients probabilistically. An adaptive sampling strategy based on the sample space partitioning in a few regions and on the Kullback–Leibler divergence

was also proposed to further improve the multi-fidelity method's performance for seismic fragility calculation. Implementing the gPCE-MFRF method and the adaptive sampling requires various computational steps to be performed, such as the definition of orthogonal basis functions and the Kullback–Leibler divergence solution. Their use is convenient when the structure under investigation is particularly complex or when the number of random variables is large, i.e. refined time-consuming analyses would be required. In all these cases, the preliminary work needed for the practical implementation of the procedures and building different structural models is negligible compared to the computational burden required by common approaches. Sets of *a-priori* values for reference parameters, such as cardinality of the gPCE and ratios between the number of analyses required for different model classes, can easily be defined against varying target accuracies.

An illustrative case study of an archetype reinforced concrete building was analysed to test the feasibility of the proposed approach. The results show a good agreement between fragility relationships derived with the proposed approach and those derived with the conventional robust fragility considering only the high-fidelity model. Furthermore, a sensitivity analysis on the most affecting parameters of the proposed adaptive sampling was carried out to provide practical consideration about their calibration. Choosing such a simple case study allows showcasing better the proposed approach and potential results and the implications of different assumptions in using such an approach.

Future studies will focus on developing practical rules to improve the applicability of the proposed multi-fidelity approach in more complex case studies. For example, structural systems of different types (e.g. bridges, dams) and buildings of other materials/lateral-load resisting systems (e.g. masonry, steel) can be analysed within a parametric framework to derive practical considerations regarding the calibration/approximation error of both the gPCE-MFRF method and the adaptive sampling approach.

ACKNOWLEDGMENTS

The authors also acknowledge the insightful comments from Prof Fatemeh Jalayer (Università degli Studi di Napoli Federico II, Italy) and two anonymous reviewers that significantly improved the quality of this study. This study was performed in the framework of the project “Dipartimenti di Eccellenza”, funded by the Italian Ministry of Education, University and Research at IUSS Pavia; and the Marie Skłodowska-Curie Research Grants Scheme MSCA-IF-2018: 843794 for Roberto Gentile, funded by the European Union’s Horizon 2020 research and innovation programme.

APPENDIX A

Bayesian view of the polynomial expansion coefficients

Once the structure of the gPCE (previous Section) is defined and L training points (i.e. analysis results $\mathbf{y}$) are available, the combination coefficients $b_{\mathbf{i}}$ (Equation 5) must be calibrated. According to [26], the gPCE coefficient calibration can be seen as an application of the Bayes rule.

Let us consider the combination coefficient vector ($\boldsymbol{b}$), with dimension $N \times 1$, composed of independent random variables. The prior distribution is then written as,

$$f(\boldsymbol{b}) = \prod_{|\mathbf{i}|\leq N} f(b_{\mathbf{i}}). \tag{15}$$

By applying the Bayes rule, the posterior distribution of the combination coefficients $f(\boldsymbol{b}|\mathbf{y})$ is derived as

$$f(\boldsymbol{b}|\mathbf{y}) \sim f(\mathbf{y}|\boldsymbol{b})\, f(\boldsymbol{b}), \tag{16}$$

where, $f(\mathbf{y}|\boldsymbol{b})$ is the likelihood function. In this study, both the prior distribution and the likelihood function are considered as normally distributed, that is

$$f(\boldsymbol{b}) \sim \exp\left(-\frac{1}{2}\|\boldsymbol{b}\|_2^2\right), \tag{17}$$

$$f(\boldsymbol{b}|\mathbf{y}) \sim \exp\left(-\frac{1}{2}\|\boldsymbol{y}-\widehat{\boldsymbol{u}}_N\|_2^2\right)\ \exp\left(-\frac{1}{2}\|\boldsymbol{b}\|_2^2\right). \quad (18)$$

In the previous equations, $\|\cdot\|_2$ is the 2-norm, and $\widehat{\boldsymbol{u}}_N$ is the vector of the surrogated quantity of interest derived through the gPCE considering the coefficients $\boldsymbol{b}$.

Normally distributed likelihood functions are commonly adopted to update numerical model parameters [27,30,60] when a large number of observations (i.e. the dimension of **y**) are available. The normality assumption of the combination coefficient prior distribution has little effect on the procedure because of the relatively large number of analysis results [12]. These two assumptions allow using conjugated Gaussian distributions, thus further reducing the computational burden. However, the resolution strategy proposed in [26] is adopted in this study to promote the sparsity of the gPCE basis (i.e. some of the combination coefficients are zero). This feature further improves the performance of the method. In fact, if the basis is sparse, most of the components of $\boldsymbol{b}^{\mathrm{MF}}$, $\boldsymbol{b}^{\mathrm{HF}}$ and $\boldsymbol{b}_j^{\mathrm{LF}}$ (Equation 10) are zero, and then the dimension of the optimisation problem shown in Equation 10 is reduced.

REFERENCES

1. Silva V, Crowley H, Varum H, Pinho R, Sousa R. Evaluation of analytical methodologies used to derive vulnerability functions. *Earthquake Engineering and Structural Dynamics* 2014. DOI: 10.1002/eqe.2337.
2. Silva V, Akkar S, Baker J, Bazzurro P, Castro JM, Crowley H, *et al.* Current Challenges and Future Trends in Analytical Fragility and Vulnerability Modeling. *Earthquake Spectra* 2019; **35**(4): 1927–1952. DOI: 10.1193/042418EQS101O.
3. Franchin P, Ragni L, Rota M, Zona A. Modelling Uncertainties of Italian Code-Conforming Structures for the Purpose of Seismic Response Analysis. *Journal of Earthquake Engineering* 2018; **22**(sup2): 1964–1989. DOI: 10.1080/13632469.2018.1527262.
4. Kiureghian A Der, Ditlevsen O. Aleatory or epistemic? Does it matter? *Structural Safety* 2009; **31**(2): 105–112. DOI: 10.1016/j.strusafe.2008.06.020.
5. Gentile R, Galasso C. Gaussian process regression for seismic fragility assessment of building portfolios. *Structural Safety* 2020; **87**(101980). DOI: 10.1016/j.strusafe.2020.101980.
6. Vamvatsikos D, Fragiadakis M. Incremental dynamic analysis for estimating seismic performance sensitivity and uncertainty. *Earthquake Engineering and Structural Dynamics* 2010; **39**(2): 141–163. DOI: 10.1002/eqe.935.
7. Jalayer F, Ebrahimian H. Seismic reliability assessment and the nonergodicity in the modelling parameter uncertainties. *Earthquake Engineering & Structural Dynamics* 2020: 1–24.
8. Liel AB, Haselton CB, Deierlein GG, Baker JW. Incorporating modeling uncertainties in the assessment of seismic collapse risk of buildings. *Structural Safety* 2009; **31**(2): 197–211.
9. Sevieri G, De Falco A, Marmo G. Shedding Light on the Effect of Uncertainties in the Seismic Fragility Analysis of Existing Concrete Dams. *Infrastructures* 2020; **5**(22).
10. Breitung K. 40 years FORM: Some new aspects? *Probabilistic Engineering Mechanics* 2015; **42**: 71–77.
11. Au SK, Beck JL. Subset Simulation and its Application to Seismic Risk Based on Dynamic Analysis. *Journal of Engineering Mechanics* 2003; **129**(8): 901–917. DOI: 10.1061/(ASCE)0733-9399(2003)129:8(901).
12. Box GEP, Tiao GC. *Bayesian Inference in Statistical Analysis*. Wiley-Interscience; 1992.
13. Jalayer F, De Risi R, Manfredi G. Bayesian Cloud Analysis: efficient structural fragility assessment using linear regression. *Bulletin of Earthquake Engineering* 2015; **13**: 1183–1203.
14. Gentile R, Galasso C. Simplicity versus accuracy trade-off in estimating seismic fragility of existing reinforced concrete buildings. *Soil Dynamics and Earthquake Engineering* 2021; **144**: 106678. DOI: 10.1016/j.soildyn.2021.106678.
15. Xiu D. *Numerical Methods for Stochastic Computations*. Princeton University Press; 2010.
16. Kullback S, Leibler RA. On information and sufficiency. *Annals of Mathematical Statistics* 1951; **22**(1): 79–86. DOI: doi:10.1214/aoms/1177729694.
17. Jalayer F, Cornell CA. Alternative non-linear demand estimation methods for probability-based seismic assessments. *Earthquake Engineering and Structural Dynamics* 2009; **38**(8): 951–972. DOI: 10.1002/eqe.876.

18. Ghanem RG, Spanos PD. *Stochastic Finite Elements: A Spectral Approach*. New York, NY: Springer New York; 1991. DOI: 10.1007/978-1-4612-3094-6.
19. Echard B, Gayton N, Lemaire M. AK-MCS: An active learning reliability method combining Kriging and Monte Carlo Simulation. *Structural Safety* 2011; **33**(2): 145–154. DOI: 10.1016/j.strusafe.2011.01.002.
20. Mai C, Konakli K, Sudret B. Seismic fragility curves for structures using non-parametric representations. *Frontiers of Structural and Civil Engineering* 2017; **11**(2): 169–186. DOI: 10.1007/s11709-017-0385-y.
21. Li M, Jia G. Multifidelity Gaussian Process Model Integrating Low- and High-Fidelity Data Considering Censoring. *Journal of Structural Engineering* 2020; **146**(3): 04019215. DOI: 10.1061/(ASCE)ST.1943-541X.0002531.
22. Xie Y, Ebad Sichani M, Padgett JE, DesRoches R. The promise of implementing machine learning in earthquake engineering: A state-of-the-art review. *Earthquake Spectra* 2020; **36**(4): 1769–1801. DOI: 10.1177/8755293020919419.
23. Wang Z, Pedroni N, Zentner I, Zio E. Seismic fragility analysis with artificial neural networks: Application to nuclear power plant equipment. *Engineering Structures* 2018; **162**: 213–225. DOI: 10.1016/j.engstruct.2018.02.024.
24. Abbiati G, Broccardo M, Abdallah I, Marelli S, Paolacci F. Seismic fragility analysis based on artificial ground motions and surrogate modeling of validated structural simulators. *Earthquake Engineering & Structural Dynamics* 2021; **50**(9): 2314–2333. DOI: 10.1002/eqe.3448.
25. Gentile R, Del Vecchio C, Pampanin S, Uva G. Refinement and validation of the Simple Lateral Mechanism Analysis (SLaMA) procedure for RC bare frames. *Journal of Earthquake Engineering* 2019: 1–29. DOI: 10.1080/13632469.2018.1560377.
26. Rosić B, Matthies HG. Sparse bayesian polynomial chaos approximations of elasto-plastic material models. *XIV International Conference on Computational Plasticity. Fundamentals and Applications*, Barcelona: 2017.
27. Gardoni P, Der Kiureghian A, Mosalam KM. *Probabilistic models and fragility estimates for bridge components and systems*. 2002.
28. Jalayer F, Ebrahimian H, Miano A, Manfredi G, Sezen H. Analytical fragility assessment using unscaled ground motion records. *Earthquake Engineering and Structural Dynamics* 2017; **46**(15): 2639–2663. DOI: 10.1002/eqe.2922.
29. Hosmer DW, Lemeshow S. *Applied Logistic Regression*. John Wiley & Sons, Inc.; 2000.
30. Sevieri G, Andreini M, De Falco A, Matthies HG. Concrete gravity dams model parameters updating using static measurements. *Engineering Structures* 2019. DOI: 10.1016/j.engstruct.2019.05.072.
31. Sevieri G, De Falco A. Dynamic Structural Health Monitoring for concrete gravity dams based on the Bayesian inference. *Journal of Civil Structural Health Monitoring* 2020; **380**.
32. Sobol' IM. Sensitivity estimates for nonlinear mathematical models. *Mathematical Modeling and Computational Experiment* 1993; **1**(4): 407–414. DOI: 1061-7590/93/04407-008.
33. Sudret B. Global sensitivity analysis using polynomial chaos expansions. *Reliability Engineering & System Safety* 2008; **93**(7): 964–979.
34. Wiener N. The Homogeneous Chaos. *American Journal of Mathematics* 1938; **60**(4): 897–936.
35. Berchier M. Multi-fidelity surrogate modelling with polynomial chaos expansions. ETH Zurich, Zurich, Switzerland, 2016.
36. Marelli S, Sudret B. *UQLab user manual - Polynomial Chaos Expansions*. 2015.
37. Bugallo MF, Elvira V, Martino L, Luengo D, Miguez J, Djuric PM. Adaptive Importance Sampling: The past, the present, and the future. *IEEE Signal Processing Magazine* 2017; **34**(4): 60–79. DOI: 10.1109/MSP.2017.2699226.
38. Huan X, Marzouk YM. Simulation-based optimal Bayesian experimental design for nonlinear systems. *Journal of Computational Physics* 2013; **232**(1): 288–317.
39. Blatman G, Sudret B. Adaptive sparse polynomial chaos expansion based on least angle regression. *Journal of Computational Physics* 2011; **230**(6): 2345–2367. DOI: 10.1016/j.jcp.2010.12.021.
40. Xiu D. *Numerical Methods for Stochastic Computations*. Princeton University Press; 2010. DOI: 10.2307/j.ctv7h0skv.
41. Gentile R, Galasso C, Idris Y, Rusydy I, Meilianda E. From rapid visual survey to multi-hazard risk prioritisation and numerical fragility of school buildings in Banda Aceh, Indonesia. *Natural Hazards and Earth System Sciences* 2019; **19**(7): 1365–1386. DOI: 10.5194/nhess-2018-397.
42. D'Ayala D, Galasso C, Nassirpour A, Adhikari RK, Yamin L, Fernandez R, *et al.* Resilient communities through safer schools. *International Journal of Disaster Risk Reduction* 2020; **45**. DOI:

10.1016/j.ijdrr.2019.101446.
43. Saputra A. Safety Performance of Concrete Structures in Indonesia. *Procedia Engineering* 2017; **171**: 985–993. DOI: 10.1016/j.proeng.2017.01.407.
44. Galasso C, Maddaloni G, Cosenza E. Uncertainly Analysis of Flexural Overstrength for Capacity Design of RC Beams. *Journal of Structural Engineering* 2014; **140**(7): 04014037.
45. Mander JB, Priestley MJN, Park R. Theoretical stress strain model for confined concrete. *Journal of Structural Engineering* 1988; **114**(8): 1804–1826.
46. King DJ, Priestley MJN, Park R. *Computer programs for concrete column design, Research Report 86/12*. Department of Civil Engineering: 1986.
47. Priestley MJN, Park R. Strength and ductility of concrete bridge columns under seismic loading. *ACI Structural Journal* 1987; **84**: 61–76.
48. Berry MP, Eberhard MO. Practical Performance Model for Bar Buckling. *Journal of Structural Engineering* 2005; **131**: 1060–1070.
49. Kowalsky MJ, Priestley MJN. Improved analytical model for shear strength of circular reinforced concrete columns in seismic regions. *ACI Structural Journal* 2000; **97**(3): 388–396.
50. International Conference of Buildings Officials (ICBO). *Uniform Building Code*. Whittier, California, USA: 1994.
51. American Society of Civil Engineers. *Minimum Design Loads and Associated Criteria for Buildings and Other Structures (ASCE/SEI 7-16)*. Reston, Virginia, USA: 2017.
52. Sevieri G, Galasso C, D'Ayala D, De Jesus R, Oreta A, Grio MEDA, *et al.* A multi-hazard risk prioritisation framework for cultural heritage assets. *Natural Hazards and Earth System Sciences* 2020; **20**(5): 1391–1414. DOI: https://doi.org/10.5194/nhess-20-1391-2020.
53. Kircher CA, Whitman R V., Holmes WT. HAZUS Earthquake Loss Estimation Methods. *Natural Hazards Review* 2006; **7**(2): 45–59. DOI: 10.1061/(asce)1527-6988(2006)7:2(45).
54. New Zealand Society for Earthquake Engineering (NZSEE). *The seismic assessment of existing buildings - technical guidelines for engineering assessments*. Wellington, New Zealand: 2017.
55. Saiidi M, Sozen M. *Simple and complex models for nonlinear seismic response of reinforced concrete structures*. Urbana, Illinois, USA: 1979.
56. Gentile R, Galasso C. Gaussian process regression for seismic fragility assessment of building portfolios. *Conference of Earthquake Risk and Engineering Towards a Resillent World*, Greenwich, UK.: 2019.
57. Freeman SA. Development and use of capacity spectrum method. *6th U.S. National Conference of Earthquake Engnineering*, Seattle: 1998.
58. Smerzini C, Galasso C, Iervolino I, Paolucci R. Ground motion record selection based on broadband spectral compatibility. *Earthq Spectra* 2014; **30**: 1427–1448. DOI: 10.1193/052312EQS197M.
59. Baker JW. Efficient analytical fragility function fitting using dynamic structural analysis. *Earthquake Spectra* 2015; **31**(1): 579–599.
60. Andreini M, Gardoni P, Pagliara S, Sassu M. Probabilistic Models for Erosion Parameters and Reliability Analysis of Earth Dams and Levees. *ASCE-ASME Journal of Risk and Uncertainty in Engineering Systems, Part A: Civil Engineering* 2016; **2**(4): 04016006. DOI: 10.1061/AJRUA6.0000878.